International Journal of Applied Science and Engineering
2013. 11, 4: 375-391

Stability Analysis of Piezoelectric FGM Plate Subjected to Electro-mechanical Loading Using Finite Element Method

Priyanka Jadhav* and Kamal Bajoria

Department of Civil Engineering, Indian Institute of Technology Bombay, Powai, Mumbai, India

Abstract: This paper investigates the stability analysis of plates made of functionally graded material (FGM) and subjected to electro-mechanical loading. A FGM plate with piezoelectric actuator and sensor at top and bottom face is considered. The material properties are assumed to be graded along the thickness direction according to simple power-law distribution in terms of the volume fraction of the constituents, while the poisson's ratio is assumed to be constant. The plate is simply supported at all edges. Using first order shear deformation theory (FOST), the finite element model is derived with von-Karman hypothesis and as a degenerated shell element. The displacement component of the present model is expanded in Taylor's series in terms of thickness co-ordinate. The governing equilibrium equation is obtained by using principle of minimum potential energy and solution for critical buckling load is obtained by solving eigenvalue problem. The stability analysis of piezoelectric FG plate is carried out to present the effect of power law index and applied mechanical pressure. Results reveal that buckling strength increases with increase in volume fraction. It can also be improved using piezo effects. The present analysis is carried out on newly introduced metal based FGM which is mixture of aluminum and stainless steel which exhibits the corrosion resistance as well as high strength property in single material.

Keywords: Finite element method; piezoelectric material; functionally graded material; first order shear deformation theory; eigen value problem; electro-mechanical loading.

1. Introduction

Functionally graded materials are the microscopically inhomogeneous composite materials which exhibits smooth and continuous change of material properties along the thickness direction. The laminated composite structures are faces major problem because of abrupt change in material properties, weakness of interfaces of layers placed between two adjacent laminates of composite structures. Such problems are overcome by using the FGM's. The advances in composite technology have lead to the increasing application of piezolaminated structure due to their sensing and actuating property also these structures have self-diagnostic and self-controlling capability. These structures can be able to control the shape, size, vibration and stability of the structural systems because of their direct and converse piezoelectric effects. Particularly the distributed piezoelectric sensor layer monitors the structural shape deformation due to the direct effect and the distributed actuator layer controls the deflection through the

* Corresponding author; e-mail: priyankajadhav@iitb.ac.in

Received 14 September 2012
Revised 10 January 2013
Accepted 10 May 2013

converse piezoelectric effect. Research on smart composite structures with integrated piezoelectric sensors and actuators have been investigated extensively. Recently researchers are focuses on thermal buckling response of ceramic-metal FGM/Piezoelectric FGM plates to control the extreme thermal environment. Praveen and Reddy [1] investigated the response of functionally graded ceramic-metal plates using a plate finite element that accounts for the transverse shear strains, rotary inertia and moderately large rotations in the von von-Karman sense. Javaheri and Eslami [2] studied buckling of functionally graded plate under influence of in-plane compressive force. Javaheri and Eslami [3] presented equilibrium and stability equations of rectangular functionally graded plate under influence of four types of thermal loading such as, uniform temperature rise, linear temperature change across the thickness, nonlinear temperature change across the thickness and linear temperature change along the length. Javaheri and Eslami [4] investigated thermal buckling of functionally graded plate based on classical plate theory and love-Kirchhoff's hypothesis. Lanhe [5] investigated thermal buckling of functionally graded moderately thick plate under two types of thermal loading such as uniform temperature rise and gradient through thickness based on first order shear deformation theory and stability equations were established. Liew et al. [6] presented thermal buckling and postbuckling analysis for moderately thick laminated rectangular plates that containing functionally graded material. Laminated Formulation was based on first order shear deformation theory, considering initial geometric imperfection. Na and Kim [7] investigated three dimensional thermal buckling analysis of functionally graded plates by using finite element method for more accurate analysis they used eighteen noded solid finite element. For maintaining kinematic stability for thin plate, strain mixed formulation was adopted considering temperature dependent material properties. Najafizadeh and Heydari [8] presented equilibrium and stability equations for circular functionally graded plate under uniform temperature rise and nonlinear temperature change across the thickness. Shariat et al. [9] investigated buckling of rectangular functionally graded plates with geometrical imperfections based on classical plate theory and they derived equilibrium, stability and compatibility equations of an imperfect functionally graded plate. Ganapathi and Prakash [10] investigated thermal buckling of simply supported functionally graded skew plates based on finite element method, Mindlin theory and eight noded serendipity element. Na and Kim [11] investigated three dimensional thermal buckling and postbuckling analysis of functionally graded plate subjected to uniform or non-uniform temperature rise by using finite element. Eighteen noded solid finite element was used for analysis. Green-Lagrange nonlinear strain-displacement relation was used for evaluation large deflection due to thermal load. Park and Kim [12] investigated thermal postbuckling and vibration control of functionally graded plates. Formulation for nonlinear finite element was based on first order shear deformation plate theory and von-Karman nonlinear strain-displacement relationship. Shariat et al. [13] presented thermal buckling of rectangular functionally graded plates subjected to three types of thermal loads as uniform temperature rise, nonlinear temperature rise through the thickness and axial temperature rise using classical plate theory. Shariat et al. [14] presented buckling analysis of rectangular thick functionally graded plates subjected to thermo-mechanical loads based on third order shear deformation plate theory and derived equilibrium and stability equations. Li et al. [15] presented nonlinear thermo-mechanical post-buckling of an imperfect functionally graded circular plate, subjected to both mechanical load and transversely non-uniform temperature rise. Governing equilibrium equations for the axisymmetrical large deformation plate was based on von-Karman thin plate theory by considering geometric imperfection. Wu et al. [16] studied the post-buckling response of the functionally graded materials plate, subjected to thermal and mechanical loadings is

obtained analytically using fast converging finite double Chebyshev polynomials. Prakash et al. [17] studied nonlinear behaviour of functionally graded skew plates under thermal load by using eight noded shear flexible plate bending finite element. The material properties are temperature dependant. Matsunaga [18] investigated thermal buckling of functionally graded plates based on two-dimensional global higher-order deformation theory. Critical temperatures of a simply supported functionally graded plate subjected to uniformly and linearly distributed temperatures across the thickness of the plates were obtained by solving eigenvalue problems. Bouazza et al. [19] investigated elastic buckling of functionally graded plate under two types of thermal loading such as uniform temperature rise and linear temperature rise through the thickness. Analysis is based on first order shear deformation and von-Karman type stability and compatibility equations are obtained. Bouazza et al. [20] presented the buckling analysis of rectangular thin functionally graded plates under uniaxial and biaxial compression is investigated using classic plate theory and Navier's solution. The Von Karman's nonlinear strain-displacement relation is used to account for buckling due to mechanical load. The analysis is based on ceramic-metal FGM plate with material variation of metal to ceramic from bottom to top of the plate. Khorshidvand et al. [21] presented the thermal buckling analysis of circular piezoelectric FGM plate. Buckling temperatures are derived for solid circular plates under uniform temperature rise, nonlinear and linear temperature variation through the thickness. Sridharan and Kim [22] investigated the feasibility of piezo-electric control of stiffened plates carrying axial compression and subject to interaction of local and overall buckling. Kargarnovin et al. [23] derived an exact solution for a two-dimensional Functionally Graded Piezoelectric Material under thermo-electro-mechanical load by using of potential function method. A new kind of piezoelectric materials, named functionally graded piezoelectric materials (FGPMs) have been introduced. FGPM is a kind of piezoelectric material with material composition and properties varying continuously along certain directions. To improve the performance of structure, researchers are focused on smart structures. Liew et al. [24] presented postbuckling behavior of piezoelectric FGM plate subject to thermo-electro-mechanical loading based on Reddy's higher-order shear deformation plate theory. Galerkin differential quadrature iteration algorithm is proposed for solution of the non-linear partial differential governing equations. Shen [25] presented the postbuckling analysis for a simply supported, shear deformable functionally graded plate with piezoelectric actuators subjected to the combined action of mechanical, electrical and thermal loads. Shen [26] also presented the thermal postbuckling analysis for a simply supported shear deformable functionally graded plate under thermal loading. The compressive postbuckling under thermal environments and thermal postbuckling due to a uniform temperature rise for a simply supported shear deformable functionally graded plate with piezoelectric fiber reinforced composite (PFRC) actuators has also been reported by Shen [27]. The above works done by Shen were based on higher order shear deformation plate theory and a two step perturbation technique was employed to determine buckling loads and postbuckling equilibrium paths. Chen et al. [28] used the element free Galerkin method to analyze buckling of piezoelectric FGM rectangular plates subjected to non-uniformly distributed loads, heat and voltage. Shariyat [29] developed finite element formulation based on a higher-order shear deformation theory to present the vibration and dynamic buckling of FGM rectangular plates with surface bonded piezoelectric sensors and actuators under the influence of thermo-electro-mechanical loading. Mirzavand and Eslami [30] presented the thermal buckling of functionally graded rectangular plates integrated with surface-bonded piezoelectric actuators. The third-order shear deformation plate theory is employed to account for the transverse shear strains. The temperature dependency of the material properties is considered. The buckling analysis of the plate under thermal

loadings is carried out using the Reitz method. They indicate that the buckling temperature difference can be controlled by applying a suitable voltage on the actuator layers. A number of works have been carried out on stability analysis of FGM/piezoelectric FGM plate subjected to thermo-electro-mechanical, thermo-mechanical loading.

To the best of authors' knowledge, no work has been reported on the stability analysis of piezoelectric FGM plate subjected to electro-mechanical loading. This paper investigates the stability analysis of FG plate integrated with piezoelectric actuator and sensor at top and bottom face subjected to electro-mechanical coupling based on finite element method and FOST, von-Karman hypothesis and degenerated shell element. Also this paper focuses to control the piezoelectric FGM plate against buckling by setting the optimum thickness of piezo layer. The present analysis is carried out on newly introduced metal based FGM material which is mixture of aluminum and stainless steel. So this FGM exhibits the corrosion resistance and high strength property in single material. The approach of our work is useful in shipping, construction as well as metal industry to overcome the corrosion resistivity and high strength properties in single material.

2. Finite-element formulation

Figure 1 shows the general layout of FGM shell element integrated with piezoelectric actuator and sensor at top and bottom surface respectively. The Figure 2 shows the geometry of eight noded isoparametric degenerated shell element [31] The displacement components of the mid-point of the normal, the nodal coordinates, global stiffness matrixes, applied force vectors etc. are referred the global coordinate system. The nodal co-ordinates system is defined by local frame of three mutually perpendicular vectors $\vec{V}_1$, $\vec{V}_2$ and $\vec{V}_3$ at each nodal point with the origin at the reference surface. $\vec{V}_{3k}$ is constructed from the co-ordinates of the top and bottom surface at the k^{th} node. $\vec{V}_{1k}$ is constructed parallel to the global x-z plane and the vector $\vec{V}_{2k}$ is perpendicular to the plane defined by $\vec{V}_{3k}$ and $\vec{V}_{1k}$. ξ–η–ζ represents the curvilinear co-ordinates. The co-ordinate ξ and η is in the middle plane of element and ζ is a linear co-ordinate in the thickness direction with $\zeta = +1$ and $\zeta = -1$ at the top and bottom surfaces respectively.

The finite element formulation is based on eight noded degenerated elements and has five degrees of freedom per node. The assumption made in the formulation as, in the FOST model, the straight normal to the middle surface remain practically straight but not necessarily normal to mid surface during the deformation.

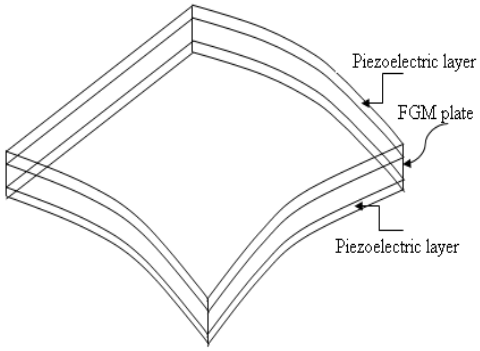

Figure 1. Piezoelectric FGM plate

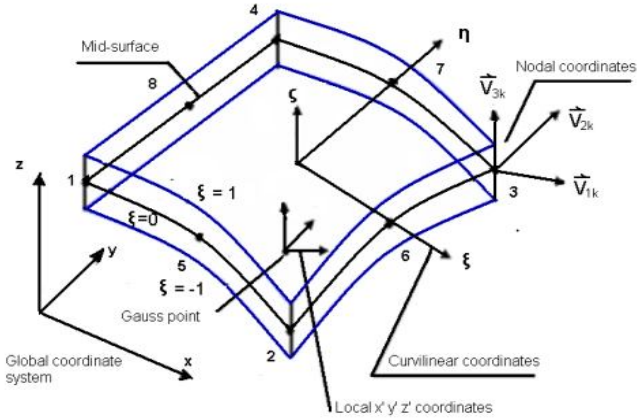

Figure 2. Geometry of an element

2.1. Element geometry and displacement field

In the isoparametric formulation co-ordinate of a point within the element are obtained as,

$$\begin{bmatrix} x \\ y \\ z \end{bmatrix} = \sum_{k=1}^{8} N_k \begin{bmatrix} x_k \\ y_k \\ z_k \end{bmatrix}_{mid} + \frac{\zeta}{2} \sum_{k=1}^{8} N_k \, t_k \begin{bmatrix} \hat{V}_{3k}^{x} \\ \hat{V}_{3k}^{y} \\ \hat{V}_{3k}^{z} \end{bmatrix} \tag{1}$$

where, $\hat{V}_{ik}^{j}\ (i=1,2,3)$ is the j^{th} component of unit vector along nodal vector $\vec{V}_{ik}$ at node k and t_k is the thickness of shell at node k. x_k, y_k and z_k are the Cartesian coordinates of the midpoint of the shell at k^{th} node. The shape function N_k at k^{th} node is expressed as,

$$N_k(\xi,\eta) = \frac{1}{4}(1+\xi\xi_k)(1+\eta\eta_k)(\xi\xi_k+\eta\eta_k-1) \qquad \text{for } k=1,2,3,4 \tag{2}$$

$$N_k(\xi,\eta) = \frac{1}{2}(1-\xi^2)(1+\eta\eta_k) \qquad \text{for } k=5,7 \tag{3}$$

$$N_k(\xi,\eta) = \frac{1}{2}(1+\xi\xi_k)(1-\eta^2) \qquad \text{for } k=6,8 \tag{4}$$

The displacement components of any point in the element are expanded in Taylor's series by using first order shear deformation theory. The displacement component of any point within element in the global co-ordinate system in terms of thickness co-ordinate for FOST is given as [32],

$$u_i = u_{mi}^{k} + \hat{V}_{1k}^{i}\, z\,\theta_y + V_{2k}^{i}\, z\,\theta_x; \qquad i=1,2,3 \text{ and } k=1,2,.....,8 \tag{5}$$

Where u_i are the displacements u, v and w (u_1=u, u_2=v and u_3=w), and u_{mi}^{k} are the displacements in the midpoint of the normal in global co-ordinate system. The Equation (5) expanded and written as,

$$\begin{Bmatrix} u \\ v \\ w \end{Bmatrix} = \sum_{k=1}^{n} N_k \begin{Bmatrix} u_{mi}^{k} \\ v_{mi}^{k} \\ w_{mi}^{k} \end{Bmatrix} + \sum_{k=1}^{n} N_k \zeta \frac{t_k}{2} \begin{bmatrix} -V_{2k}^{x} & V_{1k}^{x} \\ -V_{2k}^{y} & V_{1k}^{y} \\ -V_{2k}^{z} & V_{1k}^{z} \end{bmatrix} \begin{Bmatrix} \theta_x^k \\ \theta_y^k \end{Bmatrix} \tag{6}$$

Expressing the displacement field in a compact form,

$$\{u\} = \sum_{k=1}^{n} [N]\{d^e\} \tag{7}$$

In which $[N]=[N1, N2, ..., N_n]$ is the shape function matrix for the entire element. $\{d^e\} = \{d_1^e, ..., d_n^e\}^T$ is the element displacement vector. For the FOST model, the element displacement vector is expressed as,

$$\{d_k^e\} = \{u_m^k \quad v_m^k \quad w_m^k \quad \theta_x^k \quad \theta_y^k\}^T \tag{8}$$

Where u_m^k, v_m^k and w_m^k are the displacement components of the midpoint of the normal in the global coordinate system. θ_x^k is a positive rotation of the normal about $\vec{V}_{1k}$ and θ_y^k is a positive rotation about $\vec{V}_{2k}$.

2.2. Strain displacement relation

In this formulation linear and nonlinear strains are expressed by using von Karman assumptions, the derivatives of the u' and v' with respect to x', y' and z' are small and their square terms are neglected, also neglecting the variation of w' with z'. The Green-Lagrange strains may be expressed in local co-ordinates as,

$$\{\varepsilon'\} = \begin{Bmatrix} \varepsilon_{x'} \\ \varepsilon_{y'} \\ \gamma_{x'y'} \\ \gamma_{x'z'} \\ \gamma_{y'z'} \end{Bmatrix} = \begin{Bmatrix} \partial u'/\partial x' \\ \partial v'/\partial y' \\ \dfrac{\partial u'}{\partial y'} + \dfrac{\partial v'}{\partial x'} \\ \dfrac{\partial u'}{\partial z'} + \dfrac{\partial w'}{\partial x'} \\ \dfrac{\partial v'}{\partial z'} + \dfrac{\partial w'}{\partial y'} \end{Bmatrix} + \begin{Bmatrix} \dfrac{1}{2}\left(\dfrac{\partial w'}{\partial x'}\right)^2 \\ \dfrac{1}{2}\left(\dfrac{\partial w'}{\partial y'}\right)^2 \\ \left(\dfrac{\partial w'}{\partial y'} \cdot \dfrac{\partial w'}{\partial x'}\right) \\ 0 \\ 0 \end{Bmatrix} = \{\varepsilon'^L\} + \{\varepsilon'^{NL}\} \tag{9}$$

Where $\{\varepsilon'^L\}$ and $\{\varepsilon'^{NL}\}$ are the linear and nonlinear strain vectors respectively. $\varepsilon_{x'x'}$, $\varepsilon_{y'y'}$ and $\varepsilon_{z'z'}$ are the normal strains; $\gamma_{x'y'}$, $\gamma_{x'z'}$ and $\gamma_{y'z'}$ are the shear strains and u', v' and w' are the displacement components in the local co-ordinate system. These local derivatives are obtained from the global derivatives of the displacements u, v and w by the following operation,

$$\begin{bmatrix} \dfrac{\partial u'}{\partial x'} & \dfrac{\partial v'}{\partial x'} & \dfrac{\partial w'}{\partial x'} \\ \dfrac{\partial u'}{\partial y'} & \dfrac{\partial v'}{\partial y'} & \dfrac{\partial w'}{\partial y'} \\ \dfrac{\partial u'}{\partial z'} & \dfrac{\partial v'}{\partial z'} & \dfrac{\partial w'}{\partial z'} \end{bmatrix} = [T']^T \begin{bmatrix} \dfrac{\partial u}{\partial x} & \dfrac{\partial v}{\partial x} & \dfrac{\partial w}{\partial x} \\ \dfrac{\partial u}{\partial y} & \dfrac{\partial v}{\partial y} & \dfrac{\partial w}{\partial y} \\ \dfrac{\partial u}{\partial z} & \dfrac{\partial v}{\partial z} & \dfrac{\partial w}{\partial z} \end{bmatrix} [T'] \tag{10}$$

Where, $[T']$ is a transformation matrix given as,

$$[T'] = \begin{bmatrix} l_1 & l_2 & l_3 \\ m_1 & m_2 & m_3 \\ n_1 & n_2 & n_3 \end{bmatrix} \tag{11}$$

l_i, m_i and n_i (i=1, 2, 3) are the components of unit vectors. The relation between the derivatives of displacements in global and curvilinear co-ordinates are given by,

$$\begin{bmatrix} \frac{\partial u}{\partial x} & \frac{\partial v}{\partial x} & \frac{\partial w}{\partial x} \\ \frac{\partial u}{\partial y} & \frac{\partial v}{\partial y} & \frac{\partial w}{\partial y} \\ \frac{\partial u}{\partial z} & \frac{\partial v}{\partial z} & \frac{\partial w}{\partial z} \end{bmatrix} = J^{-1} \begin{bmatrix} \frac{\partial u}{\partial \xi} & \frac{\partial v}{\partial \xi} & \frac{\partial w}{\partial \xi} \\ \frac{\partial u}{\partial \eta} & \frac{\partial v}{\partial \eta} & \frac{\partial w}{\partial \eta} \\ \frac{\partial u}{\partial \zeta} & \frac{\partial v}{\partial \zeta} & \frac{\partial w}{\partial \zeta} \end{bmatrix} \tag{12}$$

Where J is the Jacobian matrix

$$J = \begin{bmatrix} \frac{\partial x}{\partial \xi} & \frac{\partial y}{\partial \xi} & \frac{\partial z}{\partial \xi} \\ \frac{\partial x}{\partial \eta} & \frac{\partial y}{\partial \eta} & \frac{\partial z}{\partial \eta} \\ \frac{\partial x}{\partial \zeta} & \frac{\partial y}{\partial \zeta} & \frac{\partial z}{\partial \zeta} \end{bmatrix} \tag{13}$$

The nonlinear strain vector in local co-ordinate system can be expressed using derivatives as,

$$\left\{\varepsilon^{'NL}\right\} = \frac{1}{2} \begin{bmatrix} \frac{\partial w'}{\partial x'} & 0 \\ 0 & \frac{\partial w'}{\partial y'} \\ \frac{\partial w'}{\partial y'} & \frac{\partial w'}{\partial x'} \\ 0 & 0 \\ 0 & 0 \end{bmatrix} \begin{Bmatrix} \frac{\partial w'}{\partial x'} \\ \frac{\partial w'}{\partial y'} \end{Bmatrix} = \frac{1}{2} [S][G]\left\{d^e\right\} \tag{14}$$

The matrix G is with two rows and a number of columns equal to the total number of element nodal variables. The local derivative $\frac{\partial w'}{\partial x'}$ and $\frac{\partial w'}{\partial y'}$ contains the contribution of each nodal variable (corresponding shape function derivatives) respectively. Expressing strains using strain-displacement matrices can be written as,

$$\left\{\varepsilon^{'L}\right\} = [B^{'L}]\{d^e\} \tag{15}$$

$$\left\{\varepsilon^{'NL}\right\} = \frac{1}{2}[B^{'NL}]\{d^e\} \tag{16}$$

Where, $[B^{'L}]$ and $[B^{'NL}]$ are the strain displacement matrices for the small and large strains respectively. The displacement derivatives with respect to the ξ can be expresses as,

$$\begin{Bmatrix} \frac{\partial u}{\partial \xi} \\ \frac{\partial v}{\partial \xi} \\ \frac{\partial w}{\partial \xi} \end{Bmatrix} = \sum_{k=1}^{n} N_{k,\xi} \begin{Bmatrix} u_{mi}^k \\ v_{mi}^k \\ w_{mi}^k \end{Bmatrix} + \sum_{k=1}^{n} N_{k,\xi}\, \zeta \frac{t_k}{2} \begin{bmatrix} -\partial_{2k}^x & V_{1k}^x \\ -\partial_{2k}^y & V_{1k}^y \\ -\partial_{2k}^z & V_{1k}^z \end{bmatrix} \begin{Bmatrix} \theta_x^k \\ \theta_y^k \end{Bmatrix} \tag{17}$$

The derivatives with respect to η and ζ are obtained in a similar way.

2.3. Stress-strain relations

The stress-strain relation in the local co-ordinate system can be written as,

$$\{\sigma\} = [C]\{\varepsilon\} \tag{18}$$

Where, $\{\sigma\} = \begin{bmatrix} \sigma_{xx} & \sigma_{yy} & \sigma_{xy} & \sigma_{xz} & \sigma_{yz} \end{bmatrix}^T$ is the stress vector, $\{\varepsilon\}$ is the strain vector and [C] is the elasticity matrix in global co-ordinates system. The [C] is obtained in global coordinates using the strain transformation matrix is given below [33],

$$[C] = [T_\varepsilon]^T [C'] [T_\varepsilon] \tag{19}$$

The effective material properties for FGM plates by using power law function given by [34]

$$E_f = E_{m1} V_{m1} + E_{m2} V_{m2} \tag{20}$$

$$\text{But, } V_{m1} + V_{m2} = 1 \text{ and } V_{m1} = \left(\frac{2z + h}{2h} \right)^n \tag{21}$$

$$E(z) = E_{m2} + (E_{m1} - E_{m2}) \left(\frac{2z + h}{2h} \right)^n, \qquad \text{for} - h/2 \le z \le h/2 \tag{22}$$

$$\mu(z) = \mu_{m2} + (\mu_{m1} - \mu_{m2}) \left(\frac{2z + h}{2h} \right)^n, \qquad \text{for} - h/2 \le z \le h/2 \tag{23}$$

Where, E_{m1} and E_{m2} are the elastic moduli of aluminum and stainless steel respectively, V_{m1} and V_{m2} are the volume fraction of the aluminum and stainless steel respectively, n is power law index, z is thickness coordinate variable.

2.4. Electro-mechanical coupling

The linear piezoelectric constitutive equations coupling the elastic and electric fields can be respectively expressed as the direct and the converse piezoelectric equations are given by [35, 36],

$$\{D\} = [e]\{\varepsilon\} + [g]\{E^P\} \tag{24}$$

$$\{\sigma\} = [C]\{\varepsilon\} - [e]^T \{E^P\} \tag{25}$$

Where, $\{D\}$ is the electric displacement vector, [e] is the dielectric permittivity matrix and [g] is the dielectric matrix, [E] is the electric field vector, [σ] is the stress vector and [C] is the elastic matrix for a constant electric field.

2.5. Electrical potential function

One electrical degree of freedom is used per node for each sensor and actuator layers of an element. The electric field vector is assumed to be constant over an element of the piezoelectric layer and to vary linearly through the thickness of the piezoelectric layer. The electric field strength of an element in terms of the electrical potential of the actuator and sensor layers is expressed as,

$$\left\{E_a^p\right\} = -\sum_{i=1}^{n} B_{a(i)}\,\phi_{a(i)}^e = -\left[B_a\right]\left\{\phi_a^e\right\} = -\begin{bmatrix} 0 \\ 0 \\ 1/t_a \end{bmatrix}\left\{\phi_a^e\right\} \tag{26}$$

$$\left\{E_s^p\right\} = -\sum_{i=1}^{n} B_{s(i)}\,\phi_{s(i)}^e = -\left[B_s\right]\left\{\phi_s^e\right\} = -\begin{bmatrix} 0 \\ 0 \\ 1/t_s \end{bmatrix}\left\{\phi_s^e\right\} \tag{27}$$

where t_a and t_s are the thickness of the actuator and sensor layers respectively, $\left\{\phi_a^e\right\}$ and $\left\{\phi_s^e\right\}$ are the nodal electric potential vectors for the actuator and sensor layers respectively and [B] is the field gradient matrix, can be given as follow,

$$\left\{\phi_a^e\right\} = \left\{\phi_{a1}\ \phi_{a2}\ \phi_{a3}.....\phi_{an}\right\}^T, \quad n= 1, 2, 3, ..., 8 \tag{28}$$

$$\left\{\phi_s^e\right\} = \left\{\phi_{s1}\ \phi_{s2}\ \phi_{s3}.....\phi_{sn}\right\}^T, \quad n= 1, 2, 3, ..., 8 \tag{29}$$

2.6. Potential energy and stability criteria

Total potential energy is given by,

$$\Pi^e = U^e - W^e \tag{30}$$

Where, U^e is the potential energy due to internal work done and W^e is the external work done by external forces. The internal potential energy U^e consisting of the strain energy of the entire structure and the electrical potential energy of the piezoelectric layers can be written as,

$$U^e = \frac{1}{2}\int_V \left\{\varepsilon^L\right\}^T \{\sigma\}\,dV - \frac{1}{2}\int_{V_a} \left\{E_a^p\right\}^T \{D_a\}\,dV - \frac{1}{2}\int_{V_s} \left\{E_s^p\right\}^T \{D_s\}\,dV + \int_V \left\{\varepsilon^N\right\}^T \{\sigma_0\}dV \tag{31}$$

Where, V, V_a, V_s and σ_0 are the volume of the entire structure, actuator layer, sensor layer and initial stress vector respectively. The work done by external forces due to the applied surface traction and applied electric charge on actuator is given as,

$$W^e = \int_A \left\{d^e\right\}^T [N]^T \left\{\bar{\sigma}\,(x,y)\right\} dA + \int_{A_a} \{E_a\}^T\, \bar{q}_a\,(x,y)\,dA \tag{32}$$

Where, $\bar{\sigma}(x,y)$ and $\bar{q}_a^e(x,y)$ are the surface traction vector and specified surface charge density respectively. To minimize the total potential energy, the first variation of Equation (30) is set to zero,

$$\delta\Pi^e = \delta U^e - \delta W^e = 0 \tag{33}$$

Substituting Equation (18) and (19) in Equation (31) and taking its first variation, it can be written as,

$$\begin{aligned}\left\{\delta U^e\right\} = &\int_V \left\{\delta\varepsilon^L\right\}^T [C]\left\{\varepsilon^L\right\}dV - \int_{V_a} \{\delta\varepsilon_a\}^T [e_a]^T \{E_a\}dV - \int_{V_a} \{\delta E_a\}^T [e_a]\{\varepsilon_a\}dV \\ &- \int_{V_a} \{\delta E_a\}^T [g]\{E_a\}dV - \int_{V_s} \{\delta\varepsilon_s\}^T [e_s]^T \{E_s\}dV - \int_{V_s} \{\delta E_s\}^T [e_s]\{\varepsilon_s\}dV \\ &- \int_{V_s} \{\delta E_s\}^T [g]\{E_s\}dV + \int_V \left\{\delta\varepsilon^{NL}\right\}^T \{\sigma_0\}dV\end{aligned} \tag{34}$$

$$\{\delta U^e\} = \{\delta d^e\}^T [K_d^e]\{d^e\} + \{\delta d^e\}^T [K_{da}^e]\{\phi_a^e\} + \{\delta\phi_a^e\}^T [K_{da}^e]\{d^e\} - \{\delta\phi_a^e\}^T [K_{aa}^e]\{\phi_a^e\} + \{\delta d^e\}^T [K_{ds}^e]\{\phi_s^e\} + \{\delta\phi_s^e\}^T [K_{sd}e]\{d^e\} - \{\delta\phi_s^e\}^T [K_{ss}^e]\{\phi_s^e\} + \{\delta d\}^T [K_\sigma^e]\{d\} \quad (35)$$

$$[K_\sigma^e] = \int_V [G]^T [\tau^L][G]dV \quad (36)$$

$$[\tau^L] = \begin{bmatrix} \sigma_x^L & \sigma_{xy}^L \\ \sigma_{xy}^L & \sigma_y^L \end{bmatrix} \quad (37)$$

Taking the first variation of W^e, the Equation (32) can be written as,

$$\delta W^e = \int_A \{\delta d^e\}^T [N]^T \{\bar{\sigma}(x,y)\}dA - \int_{A_a} \{\delta\phi_a^e\}^T [B_a]\,\bar{q}_a(x,y)dA \quad (38)$$

$$\delta W^e = \{\delta d^e\}^T \{F_l^e\} + \{\delta\phi_a^e\}^T \{Q_a^e\} \quad (39)$$

In which, the element mechanical force vector $\{F_l^e\}$ and the element electrical force vector $\{Q_a^e\}$ are given below

$$\{F_l^e\} = \int_A [N]^T \{\bar{\sigma}(x,y)\}dA \quad (40)$$

$$\{Q_a^e\} = -\int_v [N_a]^T q_a^e\, dA \quad (41)$$

Substituting the Equation (35) and (39) in Equation (33), and condensing the electrical degrees of freedom using static condensation the resulting equation can be written as,

$$[K^e]\{d^e\} + [K_\sigma^e]\{d^e\} = \{F_l^e\} + \{F_{ac}^e\} \quad (42)$$

$$[K^e] = [K_d^e] + [K_{da}^e][K_{aa}^e]^{-1}[K_{ad}^e] + [K_{ds}^e][K_{ss}^e]^{-1}[K_{sd}^e] \quad (43)$$

$$[K_d^e]\{d^e\} + [K_{da}^e]\{\phi_a^e\} + [K_{ds}^e]\{\phi_s^e\} = \{F_l^e\} \quad (44)$$

$$[K_{ad}^e]\{d^e\} - [K_{aa}^e]\{\phi_a^e\} = \{Q_a^e\} \quad (45)$$

$$[K_{da}^e][K_{aa}^e]^{-1}\{Q_a^e\} = \{F_{ac}^e\} \quad (46)$$

$$[K_{sd}^e]\{d^e\} - [K_{ss}^e]\{\phi_s^e\} = 0 \quad (47)$$

Where the superscript e refers to the parameter at the element level and [K] matrices with subscripts d, da, ad, aa, ds and ss are defined below

$$[K_d^e] = \int_V [B]^T [C][B]dV \quad (48)$$

$$\left[K_{da}^{e}\right]=\left[K_{ad}^{e}\right]^{T}=\int_{Va}[B]^{T}[e][B_{a}]dV \tag{49}$$

$$\left[K_{aa}^{e}\right]=\int_{Va}[B_{a}]^{T}[g][B_{a}]dV \tag{50}$$

$$\left[K_{ds}^{e}\right]=\left[K_{sd}^{e}\right]^{T}=\int_{Vs}[B]^{T}[e][B_{s}]dV \tag{51}$$

$$\left[K_{ss}^{e}\right]=\int_{Vs}[B_{s}]^{T}[g][B_{s}]dV \tag{52}$$

Assembling the element Equation (42), (44), (45) and (47) results in the global set of equations given as follows:

$$[K]\{d\}+\left[K_{\sigma}\right]\{d\}=\left\{F_{l}\right\}+\left\{F_{ac}\right\} \tag{53}$$

$$\left[K_{d}\right]\{d\}+\left[K_{da}\right]\left\{\phi_{a}\right\}+\left[K_{ds}\right]\left\{\phi_{s}\right\}=\left\{F_{l}\right\} \tag{54}$$

$$\left[K_{ad}\right]\{d\}-\left[K_{aa}\right]\left\{\phi_{a}\right\}=\left\{Q_{a}\right\} \tag{55}$$

$$\left[K_{sd}\right]\{d\}-\left[K_{ss}\right]\left\{\phi_{s}\right\}=0 \tag{56}$$

Where $\{d\}$ is the global nodal generalized displacement vector, $\left\{\phi_{a}\right\}$ and $\left\{\phi_{s}\right\}$ are the global nodal generalized electric vector for the actuator and sensor layer respectively. Equation (56) can be expressed as,

$$\left\{\phi_{s}\right\}=-[K_{ss}]^{-1}[K_{sd}]\{d\} \tag{57}$$

In case of constant gain velocity feedback control, the electrical potential to be fed back to the actuator $\left\{\phi_{a}\right\}$ is calculated as,

$$\left\{\phi_{a}\right\}=-G^{*}\left\{\phi_{s}\right\} \tag{58}$$

Where G^{*} is the feedback control gain matrix. In case of SISO (single input single output) system, the actuator and sensor voltage becomes a single value and control gain becomes a single value. The criteria for stability is obtained using the method of neutral equilibrium where the critical load is the load under which the structure can be in equilibrium both in the straight (initial) and the slightly bent configuration. $\lambda[K_{\sigma}]$ is geometric stiffness matrix based on an arbitrary reference intensity of membrane stresses. λ is a scalar multiplier which is determined such that, both the reference configuration represented by the load vector $\{d\}$ and slightly deformed $\{\{\delta\}+\{d\delta\}\}$ remains in equilibrium configuration. $\{F_{l}\}$ and $\{F_{ac}\}$ are the mechanical force vectors and resulting force vector from applied charge on actuator layer.

$$\left([K]+\lambda\left[K_{\sigma}\right]\right)\{d\}=\{F\} \tag{59}$$

$$\left([K]+\lambda\left[K_{\sigma}\right]\right)\left(\{d\}+\{\delta d\}\right)=\{F\} \tag{60}$$

Subtracting Equation (59) from Equation (60) yields the Eigen value problem

$$\left([K] + \lambda[K_\sigma]\right)\{\delta d\} = 0 \tag{61}$$

Where the critical buckling load is associated with the lowest magnitude eigenvalue and the displacement vector $\{\delta d\}$ represents the buckled mode shape.

2.7. Determination of buckling loads

The formulation presented is applicable for determining the critical values of both mechanical and electrical loads. For any specified mechanical load (P) or electrical load (q_a) the stress resultants $\{F_1\}$ or $\{F_{ac}\}$ are determined by solving Equation (53) in which the initial stresses are assumed to be zero. Using the stress resultants so obtained, the geometric stiffness matrix is obtained and the critical buckling coefficient λ_{cr} is calculated from eigenvalue analysis. The buckling load is obtained as,

Critical buckling values: For mechanical load is $P_{cr} = \lambda_{cr} P$

For electrical load is $V_{cr} = \lambda_{cr} q_a$

3. Numerical results and discussion

The stability analysis is carried out on newly introduced FGM plate which is mixture of aluminum and stainless steel and it is integrated with piezoelectric sensor and actuator. The plate is simply supported and subjected to biaxial compressions as shown in Figure 3. The material properties of FGM plate and piezoelectric layer are given in Table1. The critical buckling load is obtained following the procedure outlined in [37]. The results are presented for critical buckling load (N_{cr}) without and with piezoelectric effect and corresponding w-displacement for various volume fraction indices through the thickness without and with piezoelectric effect respectively. Since there are no appropriate comparison results available for the stability analysis of FGM plate mixture of aluminum and stainless steel, so comparison of results are done with analytical results outlined in [37] and ANSYS nonlinear analysis results for isotropic plate (In case of FGM, n=0 is assumed as isotropic plate).

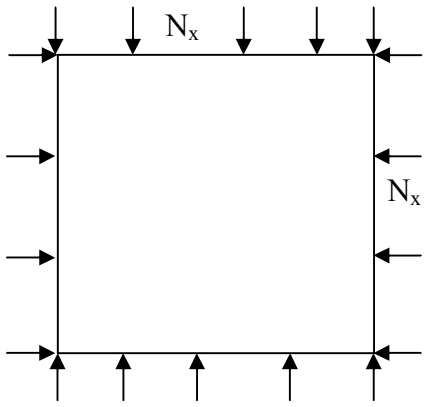

Figure 3. FGM plate subjected to biaxial compression

Table 1. Material property

E (Aluminum)	70 Gpa
E (Stainless steel)	193Gpa
Poisson's ratio	0.3
Piezostrain constants e31,e32	0.046 C/m2
Electric permittivity ε11	1.060e-10 F/m

Example 1.

Stability analysis of FGM plate having a/b=1 and b/h=1000 thickness is done. The thickness of piezoelectric sensor and actuator is 0.0012 m respectively. As per analytical method critical buckling load is calculated as 303.68 N/m for simply supported isotropic aluminum plate subjected to biaxial compression. The present analysis gives critical buckling load for (In case of FGM, n=0 is assumed as isotropic plate) of 300.009 N/m and nonlinear ANSYS finite element program gives critical buckling load is 300 N/m as shown in Figure 4. It can be seen that buckling load increases when volume fraction index increases. This is because the plate stiffness becomes strong with rise in volume fraction index. The buckling is improved with the help of piezoelectric layer which is 423.383 N/m with gain of 0.75. Figure 5 (a) and (b) shows the comparison of results for variation of w-displacement of FGM plate through the thickness for various power law index n as 0, 3, 4, 5 and 10 in case of without piezoelectric effect and with piezoelectric effect respectively. To validate the procedure, non dimensional buckling load for an isotropic plate is presented and compared with the Ref. [20], analytical solutions and ANSYS results and these have good agreement with reference, analytical solutions and ANSYS results as shown in Table 2. In this Pcr is the critical buckling load in x or y direction. In case of electro-mechanical coupling, the piezo sensor sense the deformation from structure and this can be fed back to the actuator layer and this control process is carried out by applying gain values. Table 3 and Table 4 shows the buckling load for various volume fraction indices through the thickness without and with piezoelectric effect of simply supported piezoelectric FGM plate respectively.

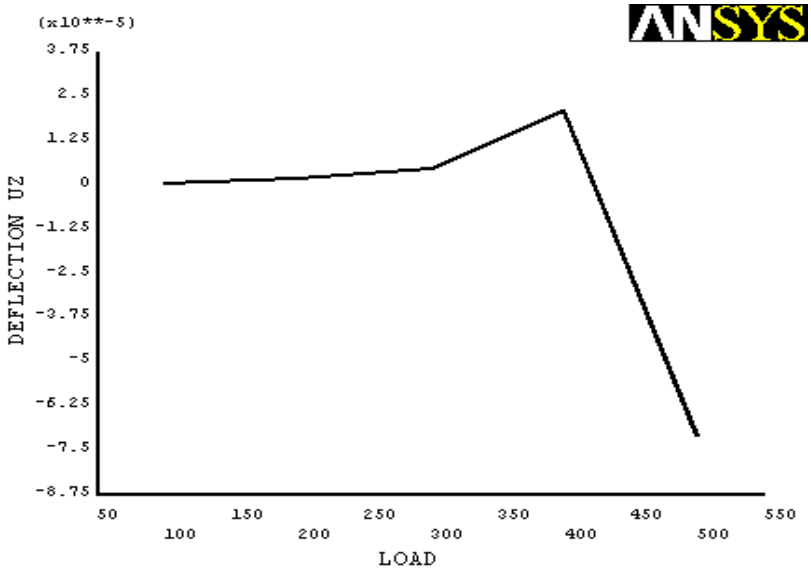

Figure 4. Load vs. w-displacement of aluminum plate subjected to biaxial compression

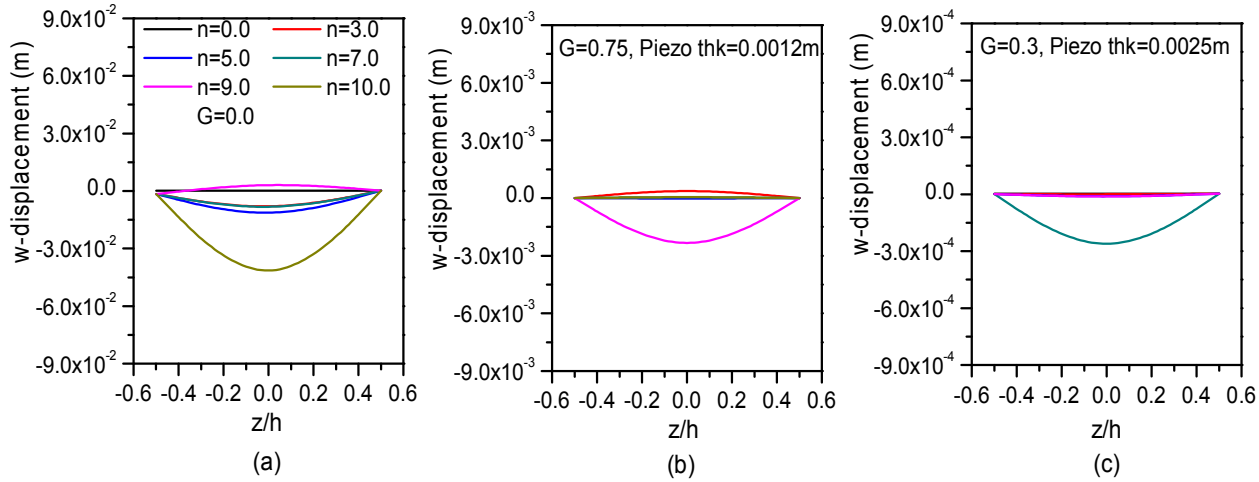

Figure 5. w-displacement vs. z/h ratio (a)without piezoeffect; (b)with piezoeffect for piezo thickness of 0.0012m; (c)without piezoeffect for piezo thickness of 0.0025m

Table 2. Comparison of the non-dimensional critical buckling load (Pcr.a2/D) for an isotropic plate (n = 0)

a/b	Ref. [14]	Analytical [35]	ANSYS	Present
1	19.7392	19.7391	19.4999	19.5006

Table 3. Buckling load (Ncr = λNx N/m) of SSSS FGM plate under biaxial compression without piezoelectric effect (FOST, b/h=1000)

z/h	n=0	n=3	n=4	n=5	n=10
0.5	300.009	300.009	300.009	300.009	300.009
0.0	300.009	343.871	356.07	375.923	389.522
-0.5	300.009	769.624	769.624	769.624	769.624

Table 4. Buckling load (Ncr = λNx N/m) of SSSS FGM plate under biaxial compression with piezoelectric effect (FOST, b/h=1000, piezo thk. = 0.0012).G*=0.75

z/h	n=0	n=3	n=4	n=5	n=10
0.5	423.383	423.383	423.383	423.383	423.383
0.0	423.383	467.923	476.081	483.052	492.656
-0.5	423.383	833.049	833.049	833.049	833.049

Example 2.

Stability analysis of FGM plate having a/b=1 and b/h=1000 thickness is done. In this example piezolayer thickness is increased to improve buckling load easily as compared to previous example. The thickness of piezoelectric sensor and actuator is 0.0025m respectively. As per analytical method critical buckling load is calculated as 303.68 N/m for simply supported isotropic aluminum plate subjected to biaxial compression. The present analysis gives critical buckling load for (In case of FGM, n=0 is assumed as isotropic plate) 300.009 N/m and nonlinear ANSYS finite element program gives critical buckling load is 300 N/m (see Figure 4).

It can be seen that buckling load increases when volume fraction index increases. This is because the plate stiffness becomes strong with rise in volume fraction index. The buckling is improved with the help of piezoelectric layer which is 428.507 N/m with gain of 0.3. As compared with results of example 1, the buckling of FGM plate can be improved easily with lower gain value and higher piezo thickness. Figure 5 (a) and (c) shows the comparison of results for variation of w-displacement of FGM plate through the thickness for various power law index n as 0, 3, 4, 5 and 10 in case of without piezoelectric effect and with piezoelectric effect respectively. Table 3 and Table 5 shows the buckling load for various volume fraction indices through the thickness without and with piezoelectric effect of simply supported piezoelectric FGM plate respectively.

Table 5. Buckling load (Ncr = λNx N/m) of SSSS FGM plate under biaxial compression with piezoelectric effect (FOST, b/h=1000, piezo thk. = 0.0025).G*=0.3

z/h	n=0	n=3	n=4	n=5	n=10
0.5	428.507	428.507	428.507	428.507	428.507
0.0	428.507	470.083	482.117	496.425	497.179
-0.5	428.507	837.120	837.120	837.120	837.120

4. Conclusions

A new model for stability analysis of piezolaminated FGM plate using finite element method and FOST is developed. The validation for the stability analysis is performed by comparing the buckling load results of FGM plate with the analytical results and ANSYS nonlinear finite element program results. Numerical studies for stability analysis using SISO control strategy suggested that buckling of FGM plate can be controlled by increasing the gain values. So buckling strength of plate can be improved by considering piezoelectric effect. Present analysis predicts that buckling strength of plate can be improved easily by using higher piezo layer thickness.

Overall results show that, buckling strength of the plate increases with increase in volume fraction indices through the thickness also the piezo thickness significantly influence the buckling control of plate with different gain values. The displacement can be improved with the help of piezoeffect using gain values. The FOST mode results closely agree with the analytical results and results of ANSYS nonlinear finite element program. It can be concluded that volume fraction index significantly influence the buckling load. In this analysis FGM exhibits the two different material properties in single material i.e. high corrosion resistivity as well as high strength. This newly introduced metal based FGM will definitely help to construction as well as metal industry.

References

[1] Praveen, G. N. and Reddy, J. N. 1998. Nonlinear Transient Thermoelastic Analysis of Functionally Graded Ceramic-Metal Plates. *International Journal of Solids Structure*, 35: 4457-4476.

[2] Javaheri, R. and Eslami, M. R. 2000. Buckling of functionally graded plates under in-plane compressive loading. *Journal of Applied Mathematics and Mechanics*, 82: 277-283.

[3] Javaheri, R. and Eslami, M. R. 2000. Thermal buckling of functionally graded plates based on higher order theory. *Journal of thermal stresses*, 25: 603-625.

[4] Javaheri, R. and Eslami, M. R. 2000. Thermal Buckling of Functionally Graded Plates. *AIAA Journal*, 40: 162-169.
[5] Lanhe, W. 2004. Thermal buckling of a simply supported moderately thick rectangular FGM plate. *Composite Structures*, 64: 211-218.
[6] Liew, K. M., Yang, J., and Kitipornchai, S. 2004. Thermal Post-Buckling of Laminated Plates Comprising Functionally Graded Materials with Temperature-Dependent Properties. *Journal of Applied Mechanics*, 71: 839-850.
[7] Na, K. S. and Kim, J. H. 2004. Three-dimensional thermal buckling analysis of functionally graded materials. *Composites: Part B*, 35: 429-437.
[8] Najafizadeh, M. M. and Heydari, H. R. 2004. Thermal buckling of functionally graded circular plates based on higher order shear deformation plate theory. *European Journal of Mechanics A/Solids*, 23: 1085-1100.
[9] Ganapathi, M. and Prakash, T. 2006. Thermal buckling of simply supported functionally graded skew plates. *Composite Structures*, 74: 247-250.
[10] Na, K. S. and Kim, J. H. 2006. Three-dimensional thermomechanical buckling analysis for functionally graded composite plates. *Composite Structures*, 73: 413-422.
[11] Park, J. S. and Kim, J. H. 2006. Thermal postbuckling and vibration analyses of functionally graded plates. *Journal of Sound and Vibration*, 289: 77-93.
[12] Shariat, B. A. S., Javaheri, R., and Eslami, M. R. 2005. Buckling of imperfect functionally graded plates under in-plane compressive loading. *Thin-Walled Structures*, 43: 1020-1036.
[13] Shariat, B. A. S. and Eslami, M. R. 2006. Thermal buckling of imperfect functionally graded plates. *International Journal of Solids and Structures*, 43: 4082-4096.
[14] Shariat, B. A. S. and Eslami M. R. 2007. Buckling of thick functionally graded plates under mechanical and thermal loads. *Composite Structures*, 78: 433-439.
[15] Li, S. R., Zhang, J. H., and Zhao, Y. G. 2007. Nonlinear thermomechanical post-buckling of circular FGM plate with geometric imperfection. *Thin-Walled Structures*, 45: 528-536.
[16] Wu, T., Shukla, K. K., and Huang, J. H. 2007. Post-buckling analysis of functionally graded rectangular plates. *Composite Structures*, 81: 1-10.
[17] Prakash, T., Singha, M. K., and Ganapathi, M. 2008. Thermal postbuckling analysis of FGM skew plates. *Engineering Structures*, 30: 22-32.
[18] Matsunaga, H. 2009. Thermal buckling of functionally graded plates according to a 2D higher-order deformation theory. *Composite Structures*, 90: 76-86.
[19] Bouazza, M., Tounsi, A., Bedia, E. A., and Megueni, A. 2010. Thermoelastic stability analysis of functionally graded plates: An analytical approach. *Computational Materials Science*, 49: 865-870.
[20] Bouazza, M., Ouinas, D., Yazid, A., and Hamouine, A. 2012. Buckling of thin plates under uniaxial and biaxial compression. *Journal of Materials Science and Engineering B*, 2: 487-492.
[21] Khorshidvand, A. R., Jabbari, M., and Eslami, M. R. 2012. Thermoelastic Buckling Analysis of Functionally Graded Circular Plates Integrated with Piezoelectric Layers. *Journal of Thermal Stresses*, 35: 695-717.
[22] Sridharan, S. and Kim. S. 2009. Piezo-electric control of stiffened panels subject to interactive buckling. *International Journal of Solids and Structures*, 46: 1527-1538.
[23] Kargarnovin, M. H., Hashemi, R., amd Emami, A. A. 2013. Electroelastic Analysis of FG Piezoelectric Structures under Thermo-Electro-Mechanical Loadings. *Mechanics of Advanced Materials and Structures*, 20: 11-27.
[24] Liew, K. M., Yang, J., and Kitipornchai, S. 2003. Postbuckling of piezoelectric FGM plates

subject to thermo-electro-mechanical loading. *International Journal of Solids and Structures*, 40: 3869-3892.
[25] Shen, H. S. 2005. Postbuckling of FGM plates with piezoelectric actuators under thermo-electro-mechanical loadings. *International Journal of Solids and Structures*, 42: 6101-6121.
[26] Shen, H. S. 2007. Thermal postbuckling behavior of shear deformable FGM plates with temperature-dependent properties. *International Journal of Mechanical Sciences*, 49: 466-478.
[27] Shen, H. S. 2009. A comparison of buckling and postbuckling behavior of FGM plates with piezoelectric fiber reinforced composite actuators. *Composite Structures*, 91: 375-384.
[28] Chen, X. L., Zhao, Z. Y., and Liew, K. M. 2008. Stability of piezoelectric FGM rectangular plates subjected to non-uniformly distributed load, heat and voltage. *Advances in Engineering Software*, 39: 2121-131.
[29] Shariyat, M. 2009. Vibration and dynamic buckling control of imperfect hybrid FGM plates with temperature-dependent material properties subjected to thermo-electro-mechanical loading conditions. *Composite Structures*, 88: 240–252.
[30] Mirzavand, B. and Eslami, M. R. 2011. A closed-form solution for thermal buckling of piezoelectric FGM rectangular plates with temperature-dependent properties. *Acta Mechanica*, 218: 87-101.
[31] Ahmad, S., Irons, B. M., and Zienkiewicz, O. C. 1970. Analysis of thick and thin shell structure by curved elements. *International Journal of Numerical Methods in Engineering*, 2: 419-51.
[32] Jadhav, P. and Bajoria, K. 2012. Stability analysis of functionally graded plate integrated with piezoelectric actuator and sensor subjected to electro-mechanical loading, *4th International Conference on Structural Stability and Dynamic*, MNIT Jaipur, India, II: 647-56.
[33] Bathe, K. J. 1996. "*Finite element procedures*". Englewood Cliffs, NJ, USA: Prentice-Hall.
[34] Javaheri, R. and Eslami, M. R. 2000. Buckling of functionally graded plates under in-plane compressive loading. *Journal of Applied Mathematics and Mechanics,* 82: 277-283.
[35] Bajoria, K. M. and Jadhav, P. A. 2013. "*Buckling of Simply Supported Piezoelectric FGM Plates Subjected to Electro-Mechanical loading using Higher-order Shear Deformation Theory*", Advanced Material Research, 622-623, 200-205. Trans Tech Publications. Switzerland.
[36] Kulkarni, S. A. and Bajoria, K. M. 2003. Finite element modeling for the smart plates/shells using higher order theory. *Composite Structures*, 62: 61-50.
[37] Timoshenko, 1970. "*Theory of elastic stability*". Tata McGraw-Hill Education.